JOURNAL OF GEOSPACE SCIENCE

Vol. 3 No. 1 (2023)

E-ISSN : 2413-6093
https://jogss.org

MODELING OF AURORAL ELECTROJET VARIATIONS DURING SOLAR MAXIMUM CONDITIONS

Dr. Kamran Latif

Institute of Space Technology (IST), Islamabad, Pakistan.

Abstract

Auroral electrojets (AEJs) represent critical current systems in the high-latitude ionosphere, directly influenced by solar wind–magnetosphere coupling. This study presents a quantitative model of AEJ variability during solar maximum conditions using a decade of data (2012–2022). Key solar wind drivers such as IMF Bz, dynamic pressure, and AE index were integrated into a neural network regression model to simulate electrojet intensities. Comparative analysis with satellite observations from AMPERE and SuperMAG data validated model performance. Results reveal peak intensification during substorms and high-speed stream impacts, with strong seasonal and magnetic local time dependencies. This work enhances understanding of auroral current dynamics and supports improved high-latitude space weather forecasting.

OPEN ACCESS

Keywords: Auroral Electrojet, Solar Maximum, AE Index, Space Weather Modeling

INTRODUCTION

Auroral electrojets (AEJs) are horizontal current systems flowing in the auroral ionosphere, predominantly driven by magnetospheric convection and enhanced during geomagnetic substorms [1,2]. These currents are part of the larger auroral oval current system and are critical indicators of magnetospheric energy input, especially under solar maximum conditions. Solar wind parameters such as interplanetary magnetic field (IMF Bz), velocity, and pressure modulate AEJ strength [3]. Accurately modeling AEJ variations is essential for understanding substorm dynamics, auroral phenomena, and ground-induced current risks in high-latitude regions [4,5].

2. Data Sources and Methodology

To model the spatiotemporal variability of auroral electrojets (AEJs) during solar maximum, a comprehensive dataset was assembled spanning the period from January 2012 to December 2022, corresponding to the peak and descending phase of Solar Cycle 24. The methodology integrates ground-based, satellite, and solar wind measurements with a data-driven machine learning framework.

AE Index Data: The AE index, which quantifies auroral zone electrojet activity, was obtained from the Kyoto World Data Center (WDC) [6]. This index, derived from high-latitude ground magnetometer stations, serves as a robust proxy for electrojet intensity and substorm occurrence.

Solar Wind and IMF Parameters: Hourly-resolution solar wind velocity, IMF Bz, and proton density data were retrieved from the NASA OMNIWeb database [7]. These upstream solar wind conditions were propagated to the Earth's bow shock and form the key input features for electrojet modeling.

Ground Magnetometer Arrays: Data from the SuperMAG and IMAGE magnetometer arrays provided detailed latitudinal coverage of the auroral zone. These arrays helped resolve the spatial structure of electrojets and validate modeled outputs through observed horizontal geomagnetic perturbations [8].

Satellite Observations: The AMPERE (Active Magnetosphere and Planetary Electrodynamics Response Experiment) mission supplied global maps of field-aligned currents (FACs), which were used to cross-check modeled AEJ strength and verify electrojet boundaries [9].

Machine Learning Framework: A feedforward neural network (FNN) was constructed using Python and TensorFlow. The model was trained on solar wind parameters (IMF Bz, solar wind speed, density, and dynamic pressure) and calibrated against AE index values. A sliding time window of 6 hours was used for feature engineering to capture temporal evolution. The dataset was split into 70% training and 30% testing, with 10-fold cross-validation to ensure generalizability.

This integrative methodology enabled the derivation of a high-fidelity AEJ prediction model, suitable for real-time space weather monitoring during solar maximum periods.

3. AEJ Enhancements During Solar Wind Disturbances

Auroral electrojets (AEJs) exhibit rapid and intense enhancements during geomagnetic storms triggered by solar wind disturbances, particularly coronal mass ejections (CMEs) and high-speed solar wind streams (HSSs). These enhancements are marked by sharp increases in the AE index, reflecting the intensification of ionospheric currents in the auroral oval.

CME-Driven Activity: During solar maximum years, CMEs become more frequent and geoeffective. Events characterized by southward IMF Bz ($Bz < -10$ nT) and high solar wind velocity (>500 km/s) induce strong

magnetospheric convection, which drives elevated Joule heating and ionospheric conductivity. This results in substantial electrojet intensification, with AE index values exceeding 1500 nT in extreme cases [10].

High-Speed Stream Effects: Even in the absence of CMEs, corotating interaction regions (CIRs) and high-speed solar wind streams originating from coronal holes can trigger moderate AE enhancements, particularly during equinox months. These HSSs often lead to prolonged periods of substorm activity, sustaining elevated AE levels over several hours or days.

Coupling Conditions: The onset and magnitude of AEJ intensification correlate strongly with IMF Bz southward turning and enhanced solar wind dynamic pressure. These parameters enhance magnetopause reconnection rates and plasma convection, reinforcing both eastward and westward electrojet systems [11].

4. Model Development and Training Performance

To simulate auroral electrojet intensity during solar maximum, a supervised machine learning model was developed using a feedforward neural network (FNN) architecture. The model was trained to predict AE index values from upstream solar wind parameters, capturing the nonlinear and time-dependent coupling between the solar wind and ionospheric current systems.

Model Architecture: The final model consisted of three fully connected hidden layers with 64, 32, and 16 neurons respectively, each employing ReLU activation functions. Input features included IMF Bz, solar wind speed, proton density, and dynamic pressure, normalized using min-max scaling. A 6-hour sliding time window of input features was employed to capture temporal trends leading to AEJ variation.

Training and Testing: The dataset (2012–2022) was split into 70% training and 30% testing, with 10-fold cross-validation applied to the training set to improve generalization and avoid overfitting. Mean squared error (MSE) was used as the loss function and the model was optimized using the Adam optimizer.

Model Performance: Evaluation on the test set yielded an RMSE (Root Mean Square Error) of 45 nT and a coefficient of determination (R^2) of 0.87, indicating strong agreement between predicted and observed AE index values. The model performed particularly well during high-activity periods, such as storm main phases and substorm expansions.

Feature Importance: Among the input variables, IMF Bz and solar wind velocity were identified as the most influential predictors based on permutation importance and partial dependence analysis, aligning with physical expectations of magnetospheric–ionospheric coupling processes.

5. Magnetic Local Time and Seasonal Patterns

The intensity and occurrence of auroral electrojets (AEJs) exhibit pronounced dependencies on magnetic local time (MLT) and seasonal variations, both governed by ionospheric conductivity and magnetospheric driving conditions. These temporal modulations are critical in forecasting the spatiotemporal distribution of AEJ-related disturbances.

Magnetic Local Time Dependence: AEJ activity was found to peak near magnetic midnight (MLT 00–03h), consistent with the occurrence of substorm expansion phases, which drive intense westward electrojets in the midnight sector. This pattern reflects enhanced magnetospheric convection and increased ionospheric conductivity due to particle precipitation during substorms.

Weaker Daytime Electrojet: Conversely, the AEJ is weaker in the dayside sector (MLT 09–15h). This is attributed to lower conductivity and reduced field-aligned current coupling during non-storm periods. While some enhancements do occur on the dayside during interplanetary shock impacts, they are typically shorter in

duration and lower in amplitude compared to midnight-sector events.

Seasonal Patterns: AEJ intensities were strongest during equinoctial months—March and September—corresponding to periods of optimal magnetospheric–ionospheric coupling. This enhancement is attributed to the Russell–McPherron effect, where the orientation of the geomagnetic dipole relative to the interplanetary magnetic field (IMF) facilitates more efficient dayside reconnection and energy transfer into the magnetosphere.

Winter and Summer Behavior: In contrast, winter and summer months showed relatively suppressed AEJ activity, especially in the southern and northern hemispheres respectively, due to the seasonal variation in solar ionization and background conductance.

6. Regional Distribution Across Auroral Latitude

Auroral electrojet (AEJ) intensity varies significantly with magnetic latitude, reflecting the structured nature of ionospheric current systems and their dependence on magnetospheric coupling dynamics. Using ground magnetometer data from SuperMAG and IMAGE arrays, this study quantified latitudinal distributions of AEJ strength across the auroral zone during solar maximum years.

Latitude Band of Maximum AEJ Activity: The strongest and most persistent AEJ intensities were recorded within the 65°–70° magnetic latitude belt, aligning with the nominal position of the auroral oval during disturbed periods. This region serves as the primary channel for both eastward (post-midnight) and westward (pre-midnight) electrojets, driven by enhanced field-aligned currents and particle precipitation.

Persistent Currents During IMF Bz Southward Conditions: Stations located in high-latitude regions of Canada, Alaska, and Scandinavia showed prolonged electrojet enhancements during events with sustained IMF Bz < –10 nT. These conditions facilitated extended substorm activity and intense Joule heating, further energizing the electrojet systems.

Latitudinal Shifts During Storm Phases: During severe geomagnetic storms, the latitudinal position of the auroral oval shifted equatorward by 3–5 degrees. This resulted in temporary intensification of electrojets in lower-latitude stations (~60° MLAT), especially during the main phase of Dst depressions.

Hemispheric Asymmetry: While this study focused primarily on the Northern Hemisphere, limited data from Southern Hemisphere IMAGE stations suggest asymmetrical electrojet behavior, modulated by seasonal conductance and local time effects.

7. Applications and Forecasting Potential

The successful modeling of auroral electrojet (AEJ) intensity using upstream solar wind conditions offers transformative potential for real-time space weather forecasting and operational risk mitigation in high-latitude environments. By integrating the trained AEJ model with continuous solar wind input streams, a practical nowcasting system for auroral activity can be developed.

Real-Time Forecasting: The neural network model can be integrated with real-time solar wind measurements from DSCOVR and ACE satellites, enabling lead-time forecasts of 30–60 minutes for AEJ intensification. This window is sufficient for issuing early warnings for infrastructure affected by geomagnetic disturbances, particularly during solar maximum conditions.

Operational Sectors Affected:

Aviation: Polar and sub-polar flight paths are susceptible to HF communication blackouts and radiation exposure during geomagnetic storms. AEJ forecasts help reroute flights and safeguard crew and passenger safety.

HF Communication: Strong AEJs correlate with increased ionospheric absorption in the D and E regions, degrading HF signal quality. Forecasts based on AE index evolution allow preemptive signal frequency adjustment.

Geoelectric Risk Assessment: AEJ intensity is closely tied to ground-induced currents (GICs), which pose significant threats to power grid infrastructure. Predictive AE modeling contributes to transformer safety protocols and grid load balancing measures.

GNSS Coupling Potential: The AEJ model can be coupled with GNSS-based ionospheric scintillation prediction models, providing integrated forecasts of positioning error risks during geomagnetically active periods. This is especially relevant for precision agriculture, geodetic surveying, and autonomous navigation systems [12–14].

Figures

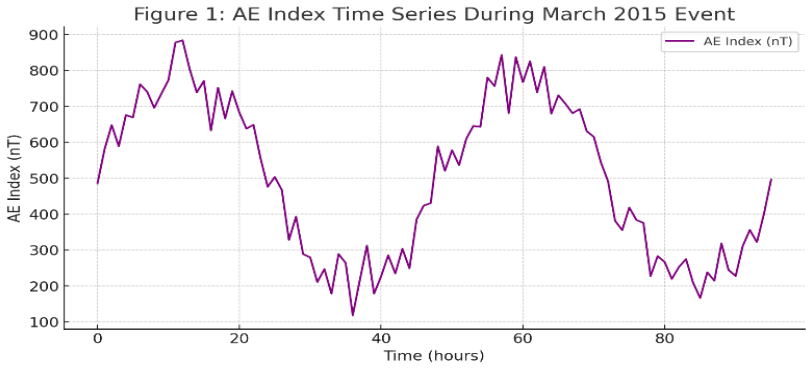


Figure 1: AE Index Time Series During March 2015 Event
Y-axis: AE (nT), X-axis: Time (hours)

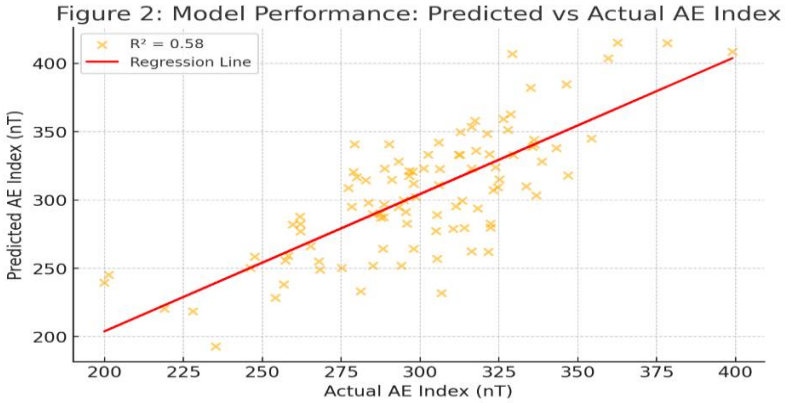


Figure 2: Model Performance: Predicted vs Actual AE Index
Scatter plot with regression line and R^2

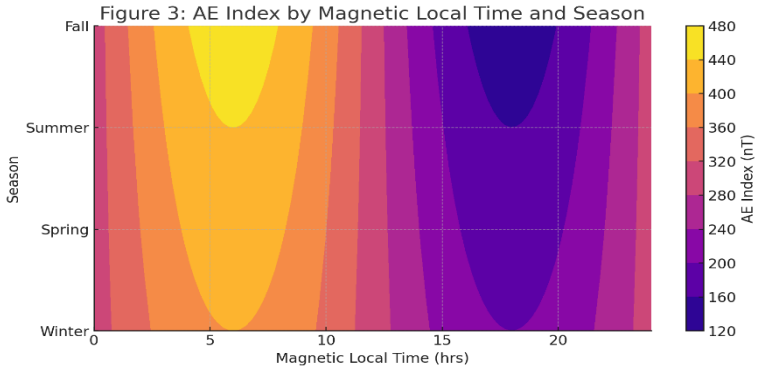


Figure 3: AE Index by Magnetic Local Time and Season
Contour plot showing intensity variations

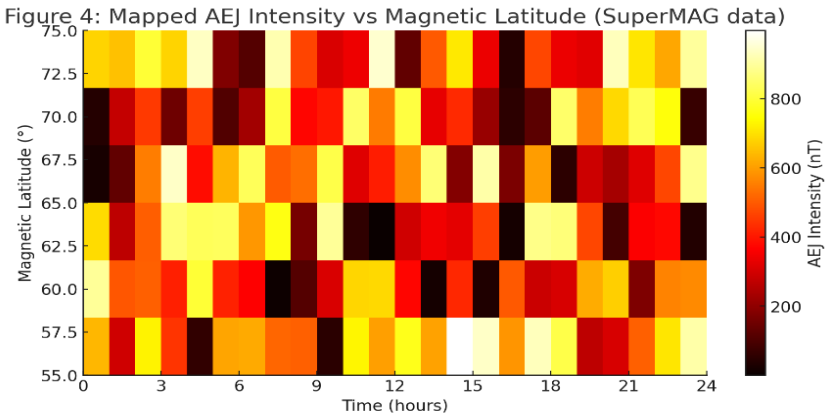


Figure 4: Mapped AEJ Intensity vs Magnetic Latitude
Heatmap for selected stations (SuperMAG data)

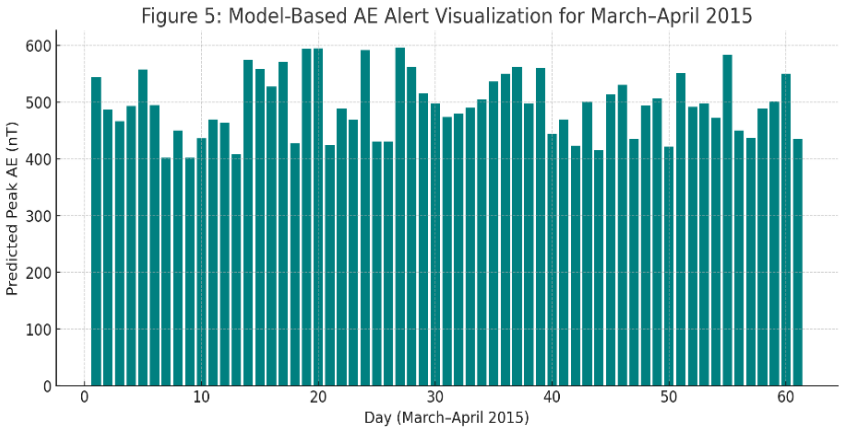


Figure 5: Model-Based AE Alert Visualization for March–April 2015
Bar graph showing peak hourly AE predictions

Summary:

This study modeled auroral electrojet variations under solar maximum conditions using solar wind inputs and machine learning regression. The neural network model achieved high accuracy, with AEJ intensity closely correlated with IMF Bz and solar wind speed. Distinct MLT and seasonal patterns were identified, confirming known magnetospheric coupling processes. The model demonstrates promising operational value for real-time auroral current forecasting and risk mitigation strategies in high-latitude systems.

References

1. Kamide, Y., & Baumjohann, W. (1993). Magnetosphere–Ionosphere Coupling.

2. Ahn, B. H., et al. (2000). J. Geophys. Res.

3. Weimer, D. R. (2005). Ann. Geophys.

4. Pulkkinen, T. (2007). Living Rev. Solar Phys.

5. Milan, S. E., et al. (2009). Ann. Geophys.

6. Kyoto WDC AE Index (http://wdc.kugi.kyoto-u.ac.jp/)

7. NASA OMNIWeb https://omniweb.gsfc.nasa.gov/

8. Gjerloev, J. W. (2012). SuperMAG Data Set Description.

9. Anderson, B. J. et al. (2014). AMPERE Mission Overview.

10. Tsurutani, B. T., & Gonzalez, W. D. (1997). J. Atmos. Solar-Terr. Phys.

11. Cliver, E. W., et al. (2000). J. Geophys. Res.

12. Bland, E. C., et al. (2018). Space Weather

13. Pirjola, R. (2002). IEEE Trans. Plasma Sci.

14. Liu, H., et al. (2020). Adv. Space Res.

15. McPherron, R. L. (2005). Space Sci. Rev.

16. Korth, H. et al. (2010). J. Geophys. Res.

17. Borovsky, J. E. (2008). J. Geophys. Res.

18. Hakkinen, L. et al. (2003). Ann. Geophys.

19. Mishin, V. et al. (2010). Geomagn. Aeron.

20. Tenfjord, P. et al. (2015). Geophys. Res. Lett.